Journal of the European Ceramic Society 21 (2001) 2739–2744

www.elsevier.com/locate/jeurceramsoc

# Raman scattering and X-ray diffraction investigations on hydrothermal barium magnesium niobate ceramics

A. Dias[a,*], V.S.T. Ciminelli[a], F.M. Matinaga[b], R.L. Moreira[b]

[a]*Departamento de Engenharia Metalúrgica e de Materiais, UFMG, Rua Espírito Santo 35, Belo Horizonte-MG, 31160-030, Brazil*
[b]*Departamento de Física, ICEx, UFMG, C.P. 702, Belo Horizonte-MG, 30123-970, Brazil*

**Abstract**

$Ba(B'_{1/3}B''_{2/3})O_3$ perovskites are important ceramic materials used as resonators in microwave technologies due to their adequate dielectric properties. These properties are mainly determined by the characteristics of the optical polar phonons of the material. A few spectroscopic investigations of lattice vibrations in $Ba(B'_{1/3}B''_{2/3})O_3$ ceramics were realized in highly ordered samples. In this work, we use Raman spectroscopy and X-ray diffraction to investigate hydrothermal $Ba(Mg_{1/3}Nb_{2/3})O_3$–BMN–ceramics with different order degree. Spectroscopic and structural data showed sensitivity to the sample microstructural evolution during sintering. Besides, they allowed independent determination of the long range order degree of the materials. The complete Raman mode assignment for the disordered and ordered BMN structure is also presented. © 2001 Elsevier Science Ltd. All rights reserved.

*Keywords:* Disordered structures; Microstructure-final; Perovskites; Powders-chemical preparation; Raman spectroscopy

## 1. Introduction

Recently, the needs of high quality dielectric resonators have grown rapidly besides the development of wireless communication. Generally, the materials used in resonators present a high dielectric constant, a high quality factor, and a small temperature coefficient of resonance frequency. The main microwave dielectrics can be found in the following systems: (i) $Ba_2Ti_9O_{20}$;[1] (ii) $(Zr,Sn)TiO_4$;[2] (iii) $BaO\text{-}Ln_2O_3\text{-}TiO_2$ ($Ln$ = La,Nd,Sm);[3] (iv) $Ba(B'_{1/3}B''_{2/3})O_3$ ($B'$ = Mg,Zn and $B''$ = Ta,Nb).[4] Among these dielectrics, the ceramics with general formula $Ba(B'_{1/3}B''_{2/3})O_3$ are currently being used as dielectric resonators for microwave and millimeter wave technologies, owing to their high permittivities and low dielectric losses (tan$\delta$).

It is well known that tan$\delta$ decreases drastically with an increase of long-range order (LRO) degree of $B$-site ions.[5] This ordering degree depends on the conditions of sample preparation,[6,7] and can be improved by annealing at very high temperatures and times.[5,8] The ability of $Ba(B'_{1/3}B''_{2/3})O_3$ perovskites to order depends also on the differences in size and valence of the two $B$-site ions: large differences favor order.[5,9] The achievement of a high LRO degree in all types of compounds predisposed to order requires that the constituent atoms are present in stoichiometric proportions, and that this ordering does not generate local charge imbalances (free-energy constraint).[10] In a previous paper, we showed that Raman spectroscopy can be used to evaluate the LRO degree of $Ba(B'_{1/3}B'_{2/3})O_3$ ceramics.[11] Now, we carried out spectroscopic and structural investigations of varying order $Ba(Mg_{1/3}Nb_{2/3})O_3$ ceramics. The disordered structure has Mg or Nb ions at the $B$ sites in a random way, while in the ordered ceramic these cations make up a stacking sequence, with the enhancing of superlattice diffraction peaks. The spectroscopic results are discussed in terms of site ordering degree and microstructural changes during sintering.

## 2. Experiment

BMN powders were produced by hydrothermal synthesis at 200 °C, for 4 h. Barium chloride hydrate, $BaCl_2.2H_2O$ (Fluka Chemie AG, Switzerland), magnesium chloride hydrate, $MgCl_2.6H_2O$ (Fluka Chemie AG, Switzerland), and niobium ammonium oxalate hydrate, $NH_4H_2[NbO(C_2O_4)_3]\cdot 3H_2O$ (CBMM, Araxá, Brazil), were used as reagents to synthesize BMN. The salts were dissolved separately in deionized water (18.2 MΩ.cm) and mixed under stirring. The niobium ammonium oxalate

* Corresponding author. Tel.: +55-31-2381817; fax: +55-31-2381815.
*E-mail address:* anderson@demet.ufmg.br (A. Dias).


PII: S0955-2219(01)00355-7

was previously treated with a sodium hydroxide solution maintained at pH > 13 and repetitively washed in order to remove the residual ammonia. After mixing, the precipitation occurred by addition of NaOH at pH = 13.5. The resultant solution was then hydrothermally treated in a *Parr* autoclave equipped with a turbine-type impeller, and heated at 4 °C/min up to the processing temperature, under saturated vapor pressure. The powders produced were washed in deionized water and dried at 80 °C. The stoichiometric proportions of the main elements and the impurity level were verified by chemical analyses.

Following, the materials were uniaxially compacted (no binder was employed) at 110 MPa into cylindrical discs of 5 mm height and 15 mm diameter. The sintering occurred in a covered alumina crucible, under heating rates of 14 °C/min, at 600, 900, 1000, 1100 and 1300 °C (±2 °C), for 4 h. X-ray powder diffraction patterns were obtained at room temperature in a Philips PW1830 diffractometer by using Cu$K_\alpha$ radiation ($\lambda = 0.15418$ nm), a graphite monochromator and a nickel filter in the $2\theta$ range 10–100° (step 0.02°$2\theta$). Scanning electron microscopy (SEM—Jeol JSM 5410) was employed to study the microstructural evolution after sintering on freshly fractured (at liquid nitrogen temperature) surfaces of the samples. The Raman scattering spectra were measured in the frequency range 60–1200 $cm^{-1}$. A Raman Jobin-Yvon T64000 triple monochromator with 1200 grooves/mm gratings coupled with a liquid nitrogen cooled CCD detector was employed. The measurements were carried out in a back scattering geometry at room temperature and using the 488 nm wavelength line of an argon laser with 50 mW power as excitation source. The surfaces of the samples were previously polished with diamond paste (9, 6 and 1 μm). The experimental resolution was better than 2 $cm^{-1}$. After a careful fitting of the Raman bands, the peak positions were determined with an accuracy of 0.2 $cm^{-1}$.

## 3. Results and discussion

The trigonal structure of the ordered BMN (space group $D^3_{3d}$) contains 15 atoms in its primitive cell with 45 degrees of freedom. Considering the vibrations at the Γ point of the 1st Brillouin zone, the ions at corresponding points of any primitive cell of the crystal move in the same way and their displacements can be expressed in terms of 45 coordinates.[11] This gives a representation which should be reduced to irreducible representations, i.e. normal modes. The symmetry operations at the Γ point belong to the $D_{3d}$ point group. The atomic positions for this structure can be found in the literature[5,9] in terms of the fractional coordinates for the hexagonal base.

The 15 ions in the BMN primitive crystalline cell can be divided into 6 groups according to the Wyckoff site designation: two Ba ions on site 2*d* and one Ba on site 1*b*; two Nb ions on sites 2*d* (ordered structures) or on sites 2*d* and 1*a* (disordered structures); one Mg on sites 1*a* (ordered) or on sites 1*a* and 2*d* (disordered structures); six oxygen ions on 6*i* sites; and three O on 3*f* sites.[5] Using group theory tools, we can establish a description of the vibrations of a Ba–Mg–Nb–O system in terms of the normal modes. As the $A_{1g}$ and $E_g$ modes are Raman-active and the $A_{2u}$ and $E_u$ modes are infrared-active, the following irreducible representations were found:[11] $7A_{2u} + 9E_u$ (infrared), $4A_{1g} + 5E_g$ (Raman), $A_{2u} + E_u$ (acoustic), $A_{2g} + 2A_{1u}$ (silent). Thus, BMN can have 9 modes that are Raman-active and 16 modes that are infrared-active. In the case of our varying LRO ceramics, we should have an average $D_{3d}$ cell, but since *B*-site ions exchange their structurally nonequivalent positions, there is an increase in the number of modes (corresponding to an enlarged number of effective atoms in the primitive cell). The presence of *B′* ions in *2d* Wyckoff sites leads to two new Raman and two new IR bands ($\Gamma_{B'/d} = A_{1g} + A_{2u} + E_g + E_u$), while the *B″* ions in *1a* site add only two new IR bands ($\Gamma_{B''/a} = A_{2u} + E_u$).

According to the above model, the ordered BMN ceramics should present 9 Raman-active modes, while the number of predicted modes for the disordered material is 11. Fig. 1 shows Raman spectra of BMN ceramics sintered at 600, 900, 1100 and 1300 °C. These spectra showed a total of 14 bands, which could be the 9 predicted modes accompanied by 5 other modes related to the order–disorder or defect induced modes. The band intensities and frequencies varied with the sintering temperature, indicating that the Raman spectra are sensitive to the variations produced by the annealing of the samples. In general, with increasing sintering temperatures the peaks become narrower and shift to higher frequency, indicating, respectively, an improvement of the LRO degree and a cell volume decreasing. An interesting peak evolution, as a function of the sintering

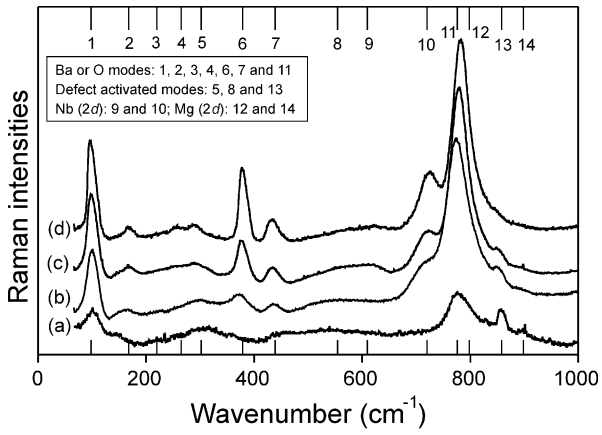


Fig. 1. Raman spectra for the BMN samples sintered at (a) 600 °C, (b) 900 °C, (c) 1100 °C and (d) 1300 °C. The 14 identified Raman modes are indicated in the figure.

temperature in the region 650–950 $cm^{-1}$, is clearly seen from a to d in Fig. 1. The bands numbered 10 and 11 intensify, while the bands 12, 13 and 14 tend to vanish.

The Raman data were fitted by Lorentzian curves, as already done in a previous study.[11] From the 14 observed bands, we attribute three bands to defect induced modes, corresponding to the bands 3 or 5, 8 and 13 (respectively located at 240, 290, 564 and 831 $cm^{-1}$ for the sample sintered at 1300 °C). These modes, besides the modes 12 and 14, are those that tend to vanish with ordering. The peaks at 794 and 919 $cm^{-1}$ (Nos. 12 and 14) can be attributed to Mg ions on 2*d*-sites and using the charge-mass general relationship $[q_{Mg}/m_{Mg}]^{1/2}/[q_{Nb}/m_{Nb}]^{1/2} = 1.24$, we identify the modes corresponding to the Nb ions as the bands 9 (625 $cm^{-1}$) and 10 (721 $cm^{-1}$). We obtained for the charge-mass relationships 1.283 and 1.274 for the peaks 9–12 and 10–14, respectively. The remaining modes should correspond to the 7 allowed bands of Ba and O ions. It is interesting to remark that these bands correspond to the incomplete set of 7 Raman bands observed by Tamura et al.[12] in the isostructural compound $Ba(Zn_{1/3}Nb_{2/3})O_3$.

The variations of the bands corresponding to order-disorder with sintering temperature can be understood by investigating the structural and microstructural changes of the samples, in particular, the quantitative changes of the LRO degree. This parameter is currently determined by X-ray techniques. Fig. 2 presents the X-ray diffraction patterns for the samples sintered at 600, 900, 1100 and 1300 °C. The LRO degree can be determined from these diffractograms in terms of the ratio of the intensity of a superstructure reflection to that of a basic unit cell reflection, as proposed by Matsumoto et al.[13] and Lu et al.[14] The ordering behavior is based on

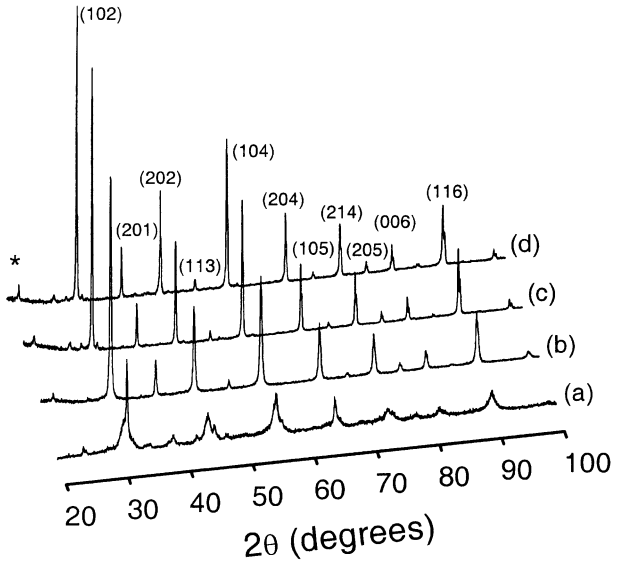


Fig. 2. X-ray powder diffractograms for the BMN ceramics sintered at (a) 600 °C, (b) 900 °C, (c) 1100 °C and (d) 1300 °C. The asterisk denotes the (100) superstructure reflection.

Warren[15] and Cullity[16] assumptions that an ordering parameter $S$ can be defined from a crystallographic point of view, by the difference between in-site and off-site ions in particular Wyckoff positions. $S$ equal to zero means a completely disordered structure, while $S$ equal to the unity means a totally ordered structure. Thus, in our case, using the above definition, the ordering parameter can be written as[14,15]

$$S = N_{Nb} - N_{Mg} = M_{Mg} - M_{Nb}, \tag{1}$$

where $N_{Nb}$ is the fraction of niobium in Nb-sites, $N_{Mg}$ is the fraction of magnesium in Nb-sites, $M_{Mg}$ is the fraction of magnesium in Mg-sites, and $M_{Nb}$ represents the fraction of niobium atoms in Mg-sites. The intensity of a X-ray diffraction peak with Miller indexes (*hkl*) can be expressed as[16]

$$I_{hkl} = kF_{hkl}^2 MLp, \tag{2}$$

where $k$ is a constant, $F_{hkl}$ is the structure factor, $M$ the multiplicity factor, and $Lp$ the Lorentz-polarization factor. For the BMN ceramics, the structure factor can be obtained as

$$\begin{aligned} F_{hkl} = &\sum f_O \exp[2\pi i(hx_i + ky_i + lz_i)] \\ &+ \sum f_{Ba} \exp[2\pi i(hx_i + ky_i + lz_i)] \\ &+ \sum \left(M_{Mg} f_{Mg} + N_{Mg} f_{Nb}\right) \exp[2\pi i(hx_i + ky_i + lz_i)] \\ &+ \sum \left(M_{Nb} f_{Mg} + N_{Nb} f_{Nb}\right) \exp[2\pi i(hx_i + ky_i + lz_i)], \end{aligned} \tag{3}$$

where $x_i, y_i, z_i$ are the positions of each ion and $f_i$ is the particular atomic scattering factor. The ordering $S$ parameter can be determined by the ratio of the intensity of the strongest superlattice reflection, (100), to the strongest peak of BST-type structure, (110). The peaks (012) and (102) are very close to (110) and should be taken into account in the calculations. The structure factors can be now evaluated for the planes (110), (102), (012) and (100) from Eqs. (3) and (1):

$$\begin{aligned} F_{110} &= 3f_{Ba} - 3f_O + \left(M_{Mg} + 2M_{Nb}\right) f_{Mg} \\ &\quad + \left(N_{Mg} + N_{Nb}\right) f_{Nb} \\ &= 3f_{Ba} - 3f_O + f_{Mg} + 2f_{Nb}; \end{aligned} \tag{4}$$

$$\begin{aligned} F_{102} &= \left(M_{Mg} - M_{Nb}\right) f_{Mg} - \left(N_{Nb} - N_{Mg}\right) f_{Nb} \\ &= \left(f_{Mg} - f_{Nb}\right) S; \end{aligned} \tag{5}$$

$$F_{012} = 3f_{Ba} - 3f_O + (M_{Mg} + 2M_{Nb})f_{Mg} + (N_{Mg} + N_{Nb})f_{Nb} = 3f_{Ba} - 3f_O + f_{Mg} + 2f_{Nb}; \quad (6)$$

$$F_{100} = (M_{Mg} - M_{Nb})f_{Mg} - (N_{Nb} - N_{Mg})f_{Nb} = (f_{Mg} - f_{Nb})S. \quad (7)$$

The atomic scattering factors ($f$), the multiplicity factors ($M$) and the Lorentz-polarization factors ($Lp$) for each diffraction peak are given by Cullity[16] and the following expressions were obtained: $F_{110} = 198.03$; $F_{102} = -24.08S$; $F_{012} = 197.97$; and $F_{100} = -26.8S$. Then, the ordering parameter $S$ can be deduced from the ratio between the X-ray intensities of Eq. (2) as

$$I_{100}/(I_{110} + I_{102} + I_{012}) = 4.3076\,S^2/(S^2 + 135.2248) \quad (8a)$$

or

$$S = [135.2248\Psi/(4.3076 - \Psi)]^{1/2}, \quad (8b)$$

where $\Psi$ is the ratio $I_{100}$ / $(I_{110} + I_{102} + I_{012})$. The above expressions allow us to calculate the occupation factors (in-site ions) $p(\mathrm{Mg}|a)$ and $p'(\mathrm{Nb}|2d)$, which are given by[5,15,16]

$$p(\mathrm{Mg}|a) = (1 - F_{Mg})S + F_{Mg},\ F_{Mg} = 1/3; \quad (9a)$$

$$p'(\mathrm{Nb}|2d) = (1 - F_{Nb})S + F_{Nb},\ F_{Nb} = 2/3. \quad (9b)$$

Let us now correlate the quantitative changes of spectroscopic and vibrational data with the sintering process. Fig. 3 shows the ordering parameter and the occupation factors calculated by Eqs. (8) and (9), the relative density and the normalized Raman intensity for the ordered Nb peaks and the disordered Mg ones as functions of the annealing temperature. A relatively high ordering degree was observed for all samples, which can be attributed to a general tendency of the hydrothermal method to produce higher ordered materials, when compared with conventional methods. As a whole, the data of Fig. 3 confirm the tendency of samples to order with sintering temperature. This result is very clear for the structural and spectroscopic data. The variations between 900 and 1100 °C are still more pronounced, leading us to believe that microstructural changes could play an important role in this temperature region and influence the ordering behavior. We note that the higher variations in the relative density were obtained exactly in the same region. In order to examine the influence of the microstructural evolutions, we have realized SEM measurements in the same samples and the results are presented below.

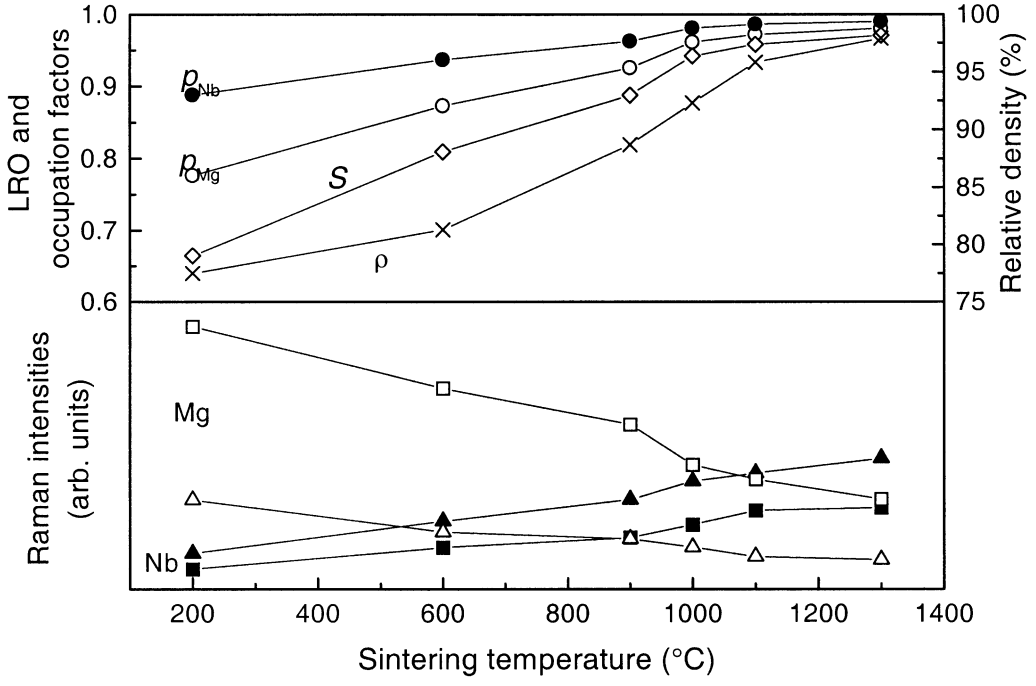


Fig. 3. Top: LRO parameter ($S$), occupation factors ($p$) and relative density (ρ); and bottom: Raman intensities for Nb (solid symbols) and Mg (open symbols) bands as functions of sintering temperature. The bands 9–12 (squares) and 10–14 (triangles) represent the modes associated to order–disorder according to the charge-mass relationship for Nb–Mg ions.

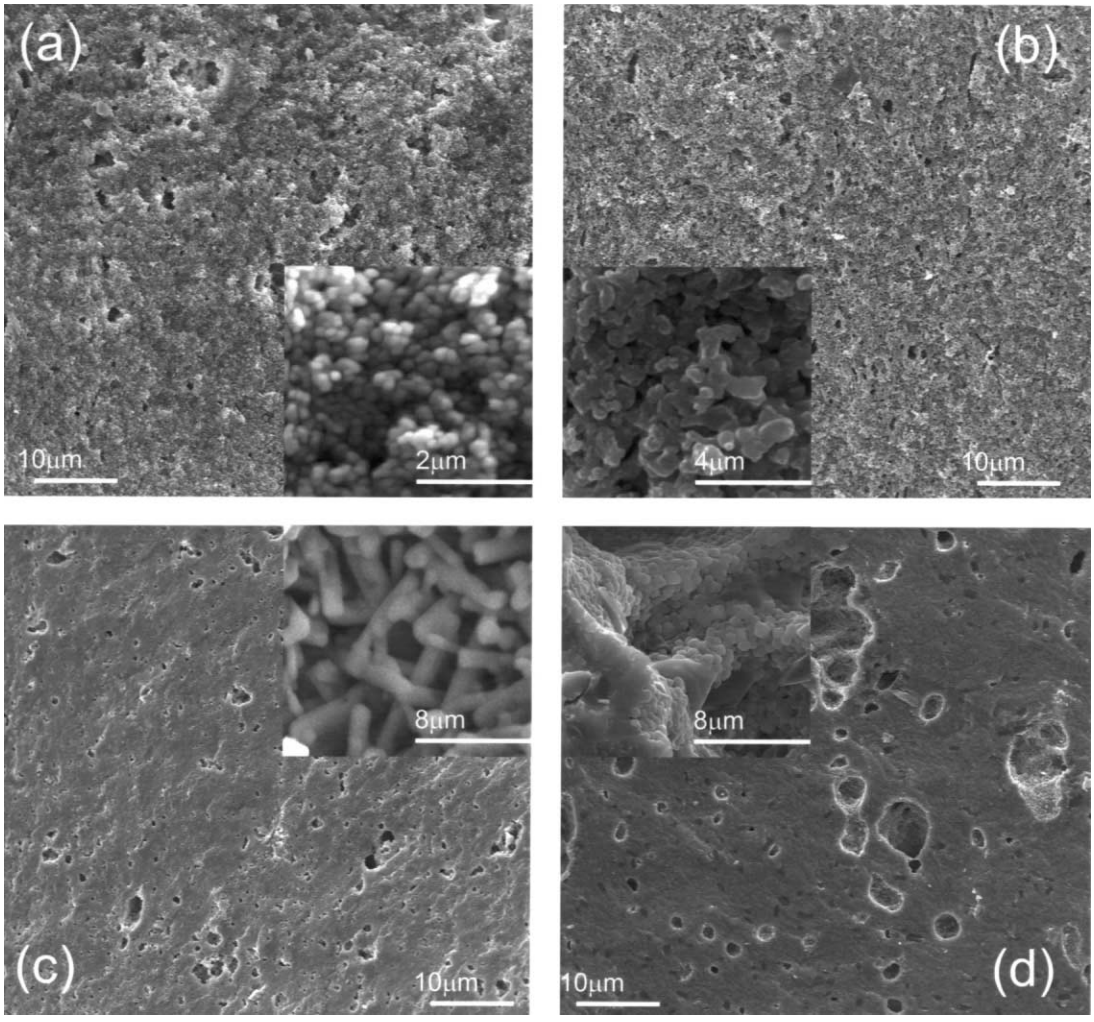


Fig. 4. SEM micrographs of the fractured surfaces of BMN sintered ceramics. (a) 900 °C, (b) 1000 °C, (c) 1100 °C and (d) 1300 °C.

Fig. 4 presents the SEM micrographs obtained on freshly fractured surfaces (at liquid nitrogen temperature) for the samples sintered at 900, 1000, 1100 and 1300 °C. These images show that the microstructure presents pores uniformly distributed in the matrix. As it can be seen, a very fine-grained microstructure was obtained after sintering at 900 and 1000 °C. The materials sintered at 1100 and 1300 °C presented larger grains and exhibited brittle fracture. For all samples, the grain size is not uniform, with small grains near the large pores and larger grains in the densified matrix. Also, two kinds of grains with different morphology exist: rounded-shape grains together with elongated ones. This type of microstructure suggests that the primary particles readily sinter and densify, promoting later grain growth, while leaving between them large pores. These large pores are difficult to eliminate even for longer times or higher sintering temperatures. For the purposes of the present work, the microstructural results of Fig. 4 besides the relative density measurements of Fig. 3 suggest that densification is the main sintering mechanism below 1000 °C, while grain growth becomes important above that temperature. Anyway, the final density correlates very well with the X-ray ordering parameter or the spectroscopic data of the pertinent bands.

Finally, Fig. 5 shows the relationship between the Raman intensities and the occupation factor for the samples studied in this work, considering the Raman ordered Nb peaks (9 and 10 of Fig. 1) and the disordered Mg ones (12 and 14 of the same figure). A very good correlation between the results obtained by the two techniques was observed (the curves have not the knee of the Fig. 3). Although the relationship between spectroscopic and structural data was not perfectly linear, this figure shows that we can evaluate the LRO degree with varying ordering samples by identifying the off-site Mg (or other $B'$) Raman modes and by controlling the vanishing of the respective bands. The microstructural evolution can also explain the linearity deviation observed for higher occupation factor values, since the densification and grain

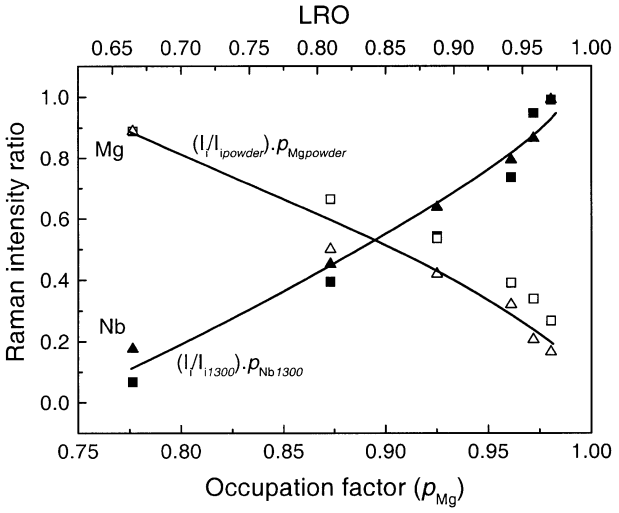


Fig. 5. Raman intensity ratios as functions of the calculated X-ray occupation factor ($p_{Mg}$) for the BMN ceramics. Same symbols as in Fig. 3.

growth processes produced a drastic microstructural change when the sintering temperature becomes higher than 1000 °C.

## 4. Conclusions

The results presented in this work represent a great advance on the understanding of the ordering behavior of $Ba(B'_{1/3}B''_{2/3})O_3$ complex perovskites. Using BMN hydrothermal ceramics as a model system, we showed that it is possible to evaluate the long-range order degree in any perovskite-type compound, through the analysis of Raman spectra. The spectroscopic data correlate very well with the structural ones and both show a strong dependence with the microstructural evolutions of the samples during sintering.

## Acknowledgements

This work was partially supported by the Brazilian agencies RHAE, CNPq, PRONEX and FAPEMIG.

## References

1. Plourde, J. K., Linn, D. F., O'Bryan, H. M. and Thomson, J., $Ba_2Ti_9O_{20}$ as a microwave dielectric resonator. *J. Am. Ceram. Soc.,* 1975, **58**, 418–420.
2. Christoffersen, R., Davies, P. K., Wei, X. H. and Negas, T., Effect of Sn substitution on cation ordering in $(Zn_{1-x}Sn_x)TiO_4$ microwave dielectric ceramics. *J. Am. Ceram. Soc.,* 1994, **77**, 1441–1450.
3. Laffez, P., Desgardin, G. and Raveau, B., Influence of calcinations, sintering and composition upon microwave properties of the $Ba_{6-x}Sm_{8+2x/3}Ti_{18}O_{54}$-type oxide. *J. Mater. Sci.,* 1992, **27**, 5229–5238.
4. Chen, X. M., Suzuki, Y. and Sato, N. J., Sinterability improvement of $Ba(Mg_{1/3}Ta_{2/3})O_3$ dielectric ceramics. *J. Mater. Sci.: Materials in Electronics,* 1994, **5**, 244–247.
5. Sagala, D. A. and Koyasu, S., Infrared reflection of $Ba(Mg_{1/3}Ta_{2/3})O_3$ ceramics. *J. Am. Ceram. Soc.,* 1993, **76**, 2433–2436.
6. Jacobson, A. J., Collins, B. M. and Fender, B. E. F., Powder neutron and X-ray diffraction determination of structure of $Ba_3Ta_2ZnO_9$-investigation of perovskite phases in system Ba-Ta-Zn-O and preparation of $Ba_2TaCdO_{5.5}$ and $BaCeInO_{5.5}$. *Acta Crystalogr. B,* 1976, **32**, 1083–1087.
7. Reaney, I. M., Petzelt, J., Voitsekhovskii, V. V., Chu, F. and Setter, N., *B*-site order and infrared reflectivity in $A(B'B'')O_3$ complex perovskite ceramics. *J. Appl. Phys.,* 1994, **76**, 2086–2092.
8. Kawashima, S., Nishida, M., Ueda, I. and Ouchi, H., $Ba(Zn_{1/3}Ta_{2/3})O_3$ ceramics with low dielectric loss at microwave-frequencies. *J. Am. Ceram. Soc.,* 1983, **66**, 421–423.
9. Galasso, F. S., *Structure, Properties and Preparation of Perovskite-Type Compounds*. Pergamon Press, Oxford, 1969 pp. 13–15, 55.
10. Kim, Y.-K., Lee, K.-M. and Jang, H. M., The B-site cation ordering and associated defect processes in $WO_3$-doped $Ba(Mg_{1/3}Ta_{2/3})O_3$. *J. Korean Phys. Soc.,* 1998, **32**, S292–S295.
11. Moreira, R. L., Matinaga, F. M. and Dias, A., Raman-spectroscopic evaluation of the long-range order in $Ba(B'_{1/3}B''_{2/3})O_3$ ceramics. *Appl. Phys. Lett.,* 2001, **78**, 428–430.
12. Tamura, H., Sagala, D. A. and Wakino, K., Lattice-vibrations of $Ba(Zn_{1/3}Ta_{2/3})O_3$ crystal with ordered perovskite structure. *Jpn. J. Appl. Phys.,* 1986, **25**, 787–791.
13. Matsumoto, K., Hiuga, T., Takada, K. and Ichimura, H., $Ba(Mg_{1/3}Ta_{2/3})O_3$ ceramics with ultra-low loss at microwave-frequencies. In *Proceedings of the 6th IEEE International Symposium on the Applications of Ferroelectrics*, IEEE, New York, 1986, p. 118.
14. Lu, C. H. and Tsai, C. C., Reaction kinetics, sintering characteristics, and ordering behavior of microwave dielectrics: barium magnesium tantalate. *J. Mater. Res.,* 1996, **11**, 1219–1227.
15. Warren, B. E., *X-Ray Diffraction*. Dover Publication, New York, 1969 p. 208.
16. Cullity, B. D., *Elements of X-Ray Diffraction*. Addison-Wesley Publishing, Reading, MA, 1978 pp. 139, 520 and 524.